MadGolem:
automatized next-to-leading order calculations for BSM

Kentarou Mawatari

Vrije Universiteit Brussel

arXiv:1108.1250

Automized Squark–Neutralino Production to Next-to-Leading Order

Thomas Binoth*,[1] Dorival Gonçalves Netto,[2] David López-Val,[2]
Kentarou Mawatari,[3,4] Tilman Plehn,[2] and Ioan Wigmore[1]

[1]*SUPA, School of Physics & Astronomy, The University of Edinburgh, UK*
[2]*Institut für Theoretische Physik, Universität Heidelberg, Germany*
[3]*Theoretische Natuurkunde and IIHE/ELEM, Vrije Universiteit Brussel, Belgium*
[4]*International Solvay Institutes, Brussels, Belgium*

(Dated: August 8, 2011)

IPMU-YITP Workshop on MC Tools for LHC @YITP, 10/09/2011

New phenomenology group at the Vrije U. Brussel

- A 5-year GOA (Geconcentreerde Onderzoeksactie) project on "Supersymmetric models and their signatures at the LHC"
  - Ben Craps, Alexander Sevrin, Alberto Mariotti (theory)
  - Catherine De Clercq [IceCube], Jorgen D'Hondt [CMS] (experiment)
  - Fabio Maltoni (pheno) - UCL/CP3
- The main goal of the project is
  - to establish a complete chain from fundamental theory to experiment.
  - to use this chain to study possible signatures of SUSY models at the LHC.
- New phenomenology members since last fall
  - Kentarou Mawatari (from U. Heidelberg) -Project leader
  - Phillip Grajek (from KEK, Japan) -PD
  - Bettina Oexl (from U. Tuebingen) -PhD
- Contact to
  - http://we.vub.ac.be/dntk/GOA.html
  - pheno@vub.ac.be / kentarou.mawatari@vub.ac.be

Outlines

- Motivation
- NLO cross sections
- MadGolem
- Squark-neutralino productions at the LHC
- Summary and outlook
- (5-min tutorial)

SUSY search at the LHC

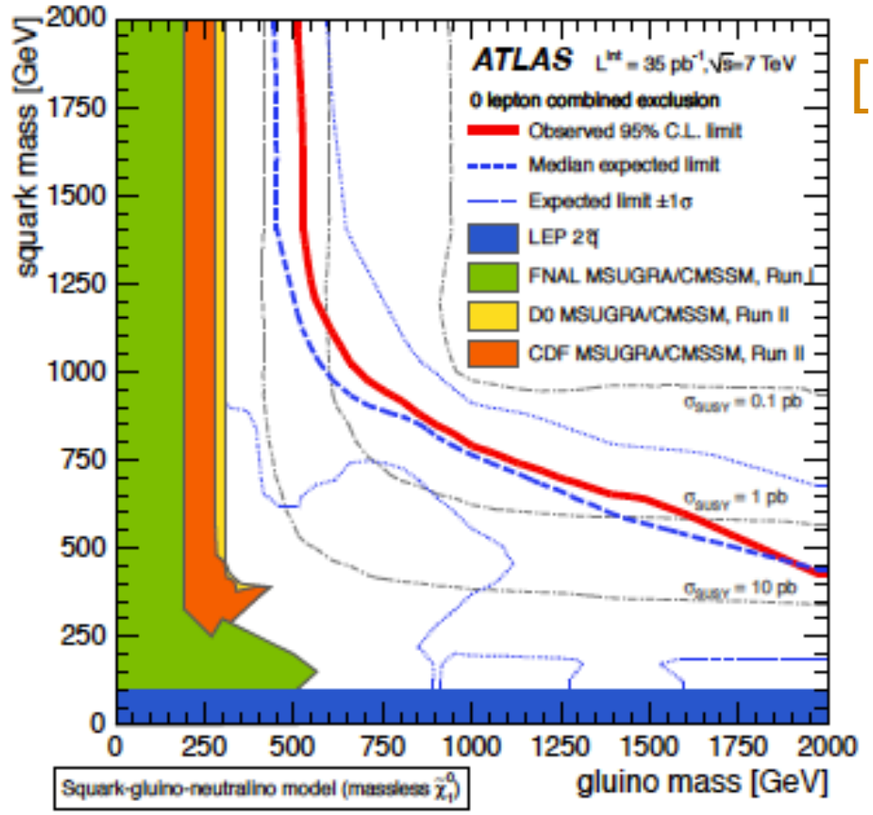

[1102.5290]

Figure 2: 95% C.L. exclusion limits in the $(m_{\tilde{g}}, m_{\tilde{q}})$ plane together with existing limits [4]. Comparison with existing limits is illustrative only as some are derived in the context of MSUGRA/CMSSM or may not assume $m_{\tilde{\chi}_1^0} = 0$.

ing the exact LO ME for up to $2 \rightarrow 5$ partons. The normalisation of these samples was fixed by a scaling designed to achieve a match to data in control regions obtained by reversing the $\Delta\phi$ requirements. After this scaling, both sets of simulations were in agreement within the experimental uncertainties, and therefore only PYTHIA QCD simulations are used further in this analysis. The resulting QCD simulation was found to be consistent with a data-driven QCD estimate in which high $E_{\mathrm{T}}^{\mathrm{miss}}$ events were generated from data by smearing low $E_{\mathrm{T}}^{\mathrm{miss}}$ events on a jet-by-jet basis with measured jet energy resolution functions. This latter technique has no MC dependencies; it provides a completely independent determination of the QCD background using only quantities measured from the data. Additional control regions having reversed $E_{\mathrm{T}}^{\mathrm{miss}}/m_{\mathrm{eff}}$ requirements were used as further checks on the normalisation.

Supersymmetric events were generated with HERWIG++ [19] v2.4.2. These samples were normalised using NLO cross sections determined by PROSPINO [20] v2.1.

SUSY search at the LHC

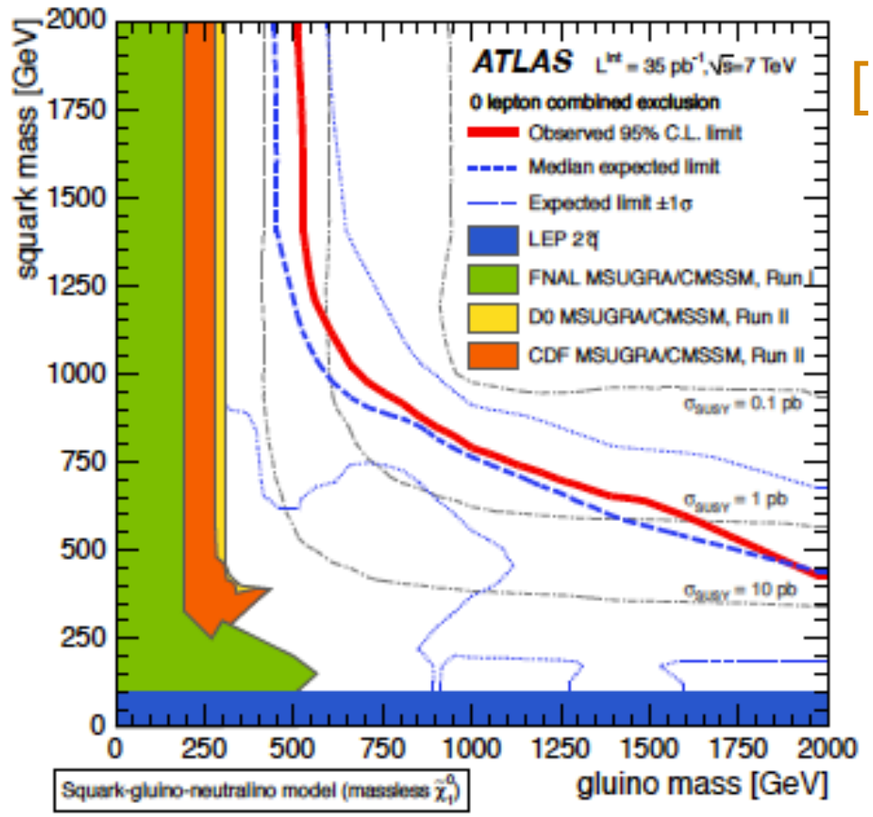

[1102.5290]

Figure 2: 95% C.L. exclusion limits in the $(m_{\tilde{g}}, m_{\tilde{q}})$ plane together with existing limits [4]. Comparison with existing limits is illustrative only as some are derived in the context of MSUGRA/CMSSM or may not assume $m_{\tilde{\chi}_1^0} = 0$.

ing the exact LO ME for up to $2 \rightarrow 5$ partons. The normalisation of these samples was fixed by a scaling designed to achieve a match to data in control regions obtained by reversing the $\Delta\phi$ requirements. After this scaling, both sets of simulations were in agreement within the experimental uncertainties, and therefore only PYTHIA QCD simulations are used further in this analysis. The resulting QCD simulation was found to be consistent with a data-driven QCD estimate in which high $E_{\mathrm{T}}^{\mathrm{miss}}$ events were generated from data by smearing low $E_{\mathrm{T}}^{\mathrm{miss}}$ events on a jet-by-jet basis with measured jet energy resolution functions. This latter technique has no MC dependencies; it provides a completely independent determination of the QCD background using only quantities measured from the data. Additional control regions having reversed $E_{\mathrm{T}}^{\mathrm{miss}}/m_{\mathrm{eff}}$ requirements were used as further checks on the normalisation.

Supersymmetric events were generated with HERWIG++ [19] v2.4.2. These samples were normalised using NLO cross sections determined by PROSPINO [20] v2.1.

SUSY search at the LHC

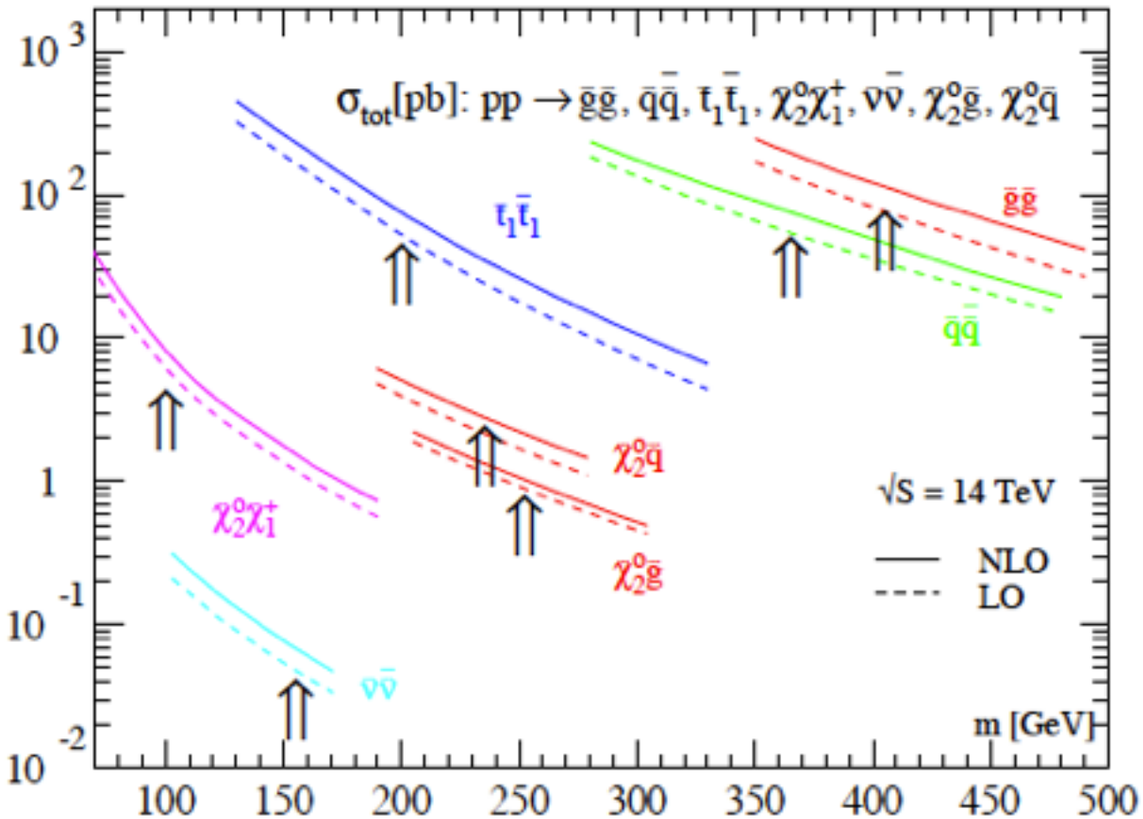

public SUSY cross sections (LO and NLO): Prospino2.1

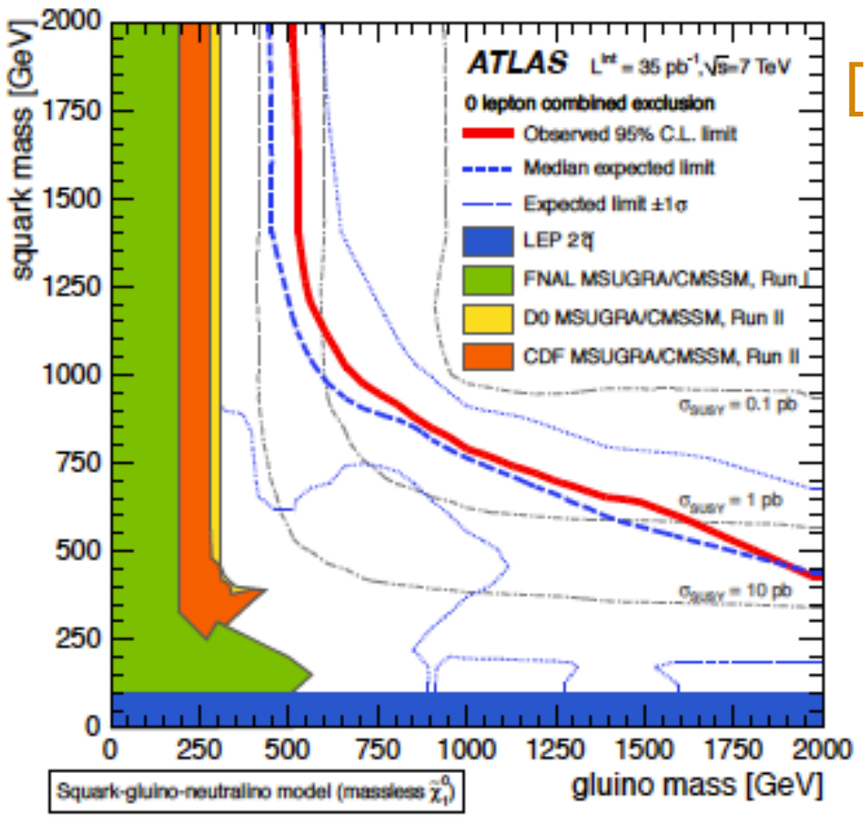

[1102.5290]

Figure 2: 95% C.L. exclusion limits in the $(m_{\tilde{g}}, m_{\tilde{q}})$ plane together with existing limits [4]. Comparison with existing limits is illustrative only as some are derived in the context of MSUGRA/CMSSM or may not assume $m_{\tilde{\chi}_1^0} = 0$.

ing the exact LO ME for up to $2 \to 5$ partons. The normalisation of these samples was fixed by a scaling designed to achieve a match to data in control regions obtained by reversing the $\Delta\phi$ requirements. After this scaling, both sets of simulations were in agreement within the experimental uncertainties, and therefore only PYTHIA QCD simulations are used further in this analysis. The resulting QCD simulation was found to be consistent with a data-driven QCD estimate in which high $E_{\mathrm{T}}^{\mathrm{miss}}$ events were generated from data by smearing low $E_{\mathrm{T}}^{\mathrm{miss}}$ events on a jet-by-jet basis with measured jet energy resolution functions. This latter technique has no MC dependencies; it provides a completely independent determination of the QCD background using only quantities measured from the data. Additional control regions having reversed $E_{\mathrm{T}}^{\mathrm{miss}}/m_{\mathrm{eff}}$ requirements were used as further checks on the normalisation.

Supersymmetric events were generated with HERWIG++ [19] v2.4.2. These samples were normalised using NLO cross sections determined by PROSPINO [20] v2.1.

SUSY search at the LHC

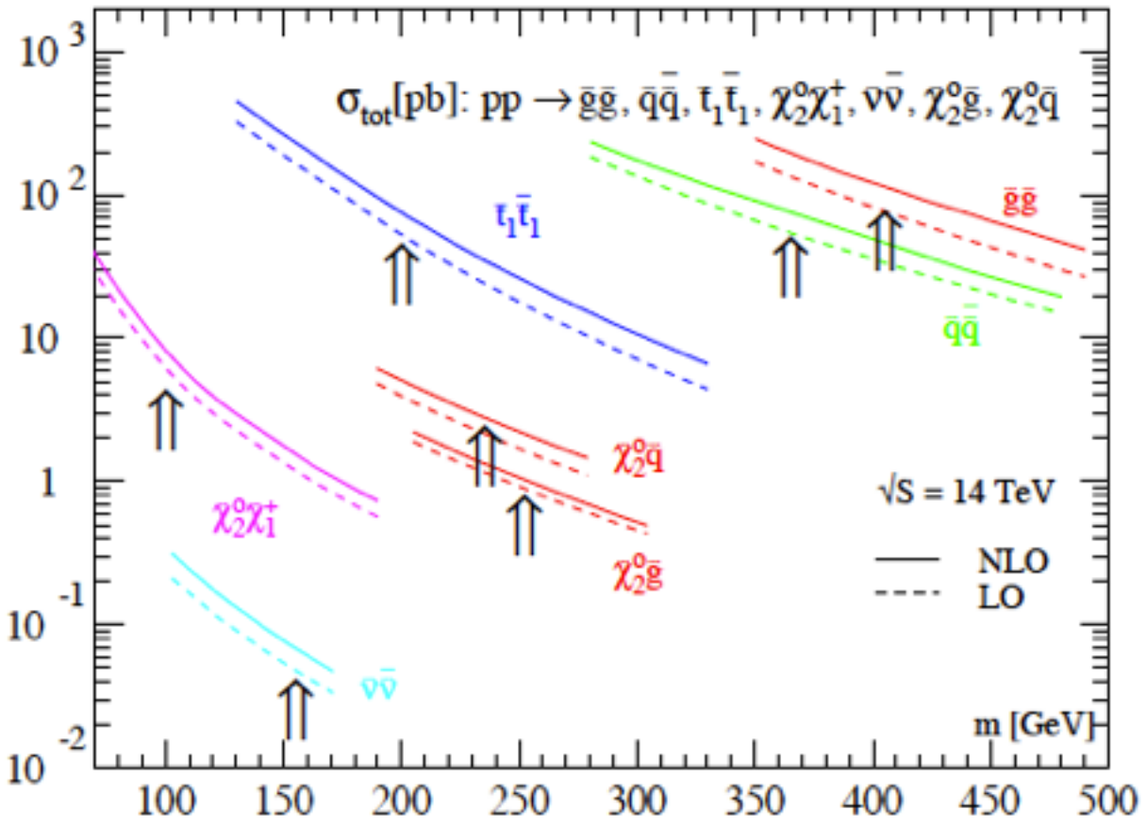

public SUSY cross sections (LO and NLO): Prospino2.1

$K = \sigma_{NLO}/\sigma_{LO} \sim 1.2$ - 1.5

Accurate NLO prediction is required.

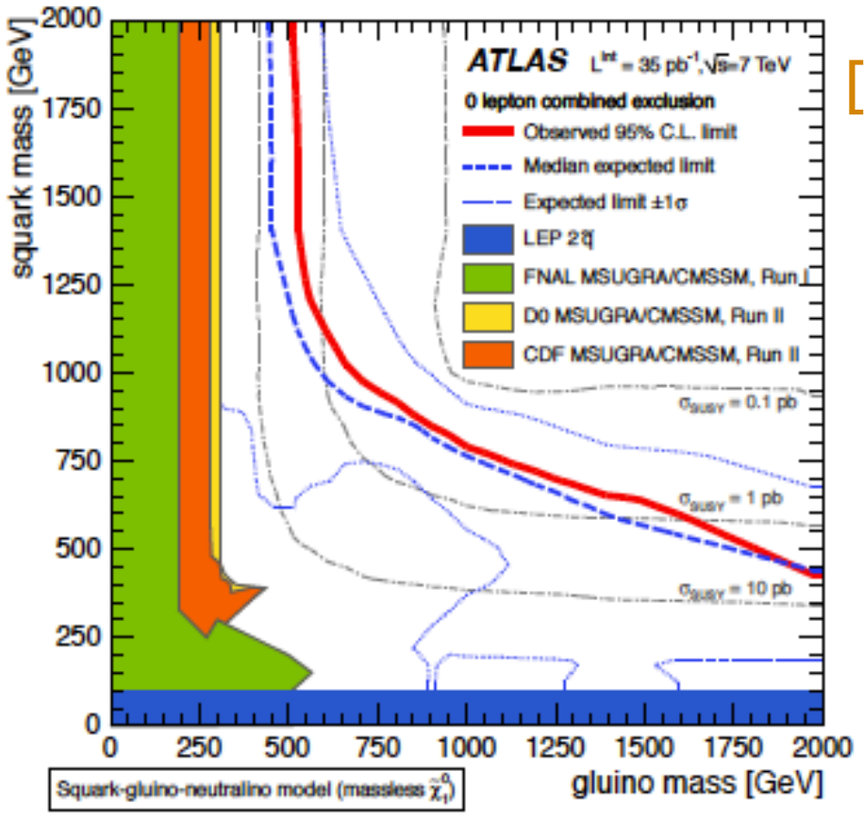

[1102.5290]

Figure 2: 95% C.L. exclusion limits in the $(m_{\tilde{g}}, m_{\tilde{q}})$ plane together with existing limits [4]. Comparison with existing limits is illustrative only as some are derived in the context of MSUGRA/CMSSM or may not assume $m_{\tilde{\chi}_1^0} = 0$.

ing the exact LO ME for up to $2 \to 5$ partons. The normalisation of these samples was fixed by a scaling designed to achieve a match to data in control regions obtained by reversing the $\Delta\phi$ requirements. After this scaling, both sets of simulations were in agreement within the experimental uncertainties, and therefore only PYTHIA QCD simulations are used further in this analysis. The resulting QCD simulation was found to be consistent with a data-driven QCD estimate in which high $E_{\mathrm{T}}^{\mathrm{miss}}$ events were generated from data by smearing low $E_{\mathrm{T}}^{\mathrm{miss}}$ events on a jet-by-jet basis with measured jet energy resolution functions. This latter technique has no MC dependencies; it provides a completely independent determination of the QCD background using only quantities measured from the data. Additional control regions having reversed $E_{\mathrm{T}}^{\mathrm{miss}}/m_{\mathrm{eff}}$ requirements were used as further checks on the normalisation.

Supersymmetric events were generated with HERWIG++ [19] v2.4.2. These samples were normalised using NLO cross sections determined by PROSPINO [20] v2.1.

PROSPINO

- PROSPINO [Beenakker, Höpker, Krämer, Plehn, Spira, Zerwas]
  = PROduction of Supersymmetric Particles in Next-to-leading Order
- the only public code to compute the SUSY NLO cross sections
- e.g. squark-gluino productions [hep-ph/9610490]

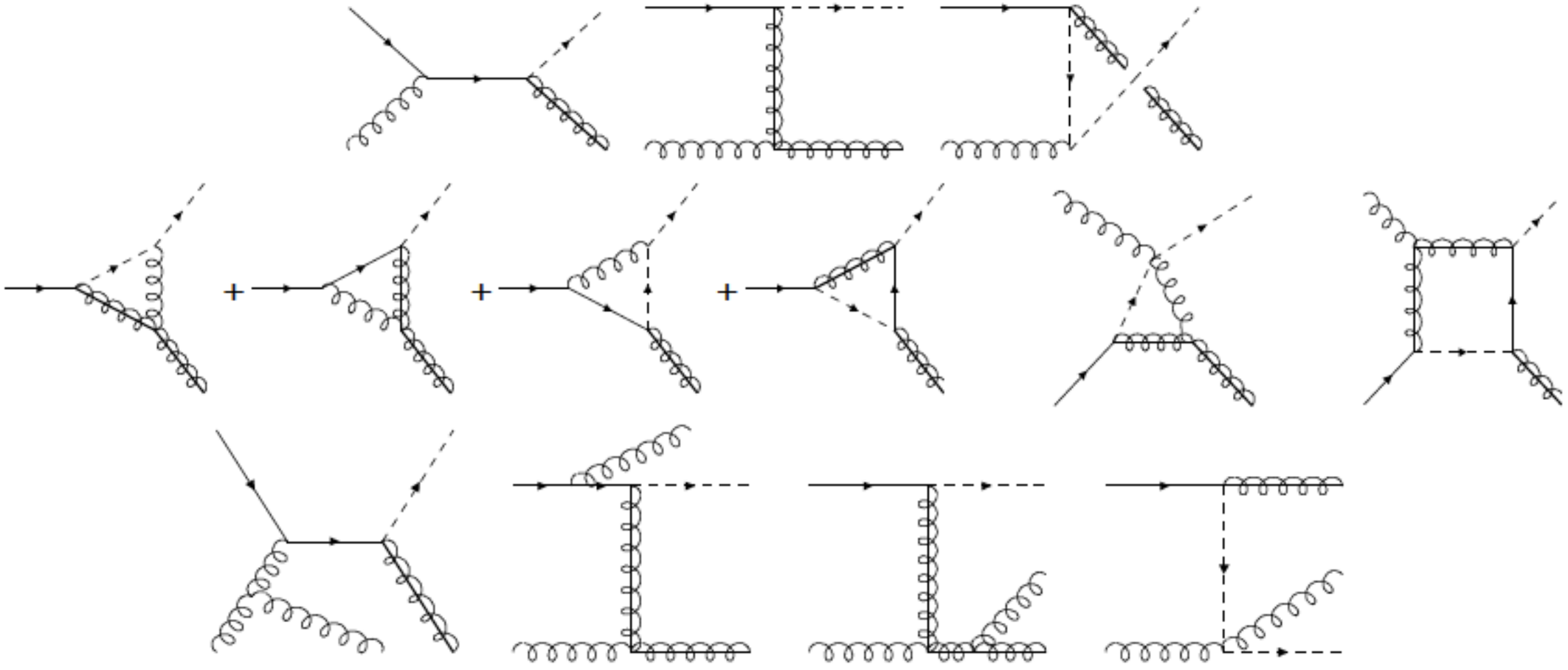

Beyond PROSPINO

- hand-coded, process dependent, user-unfriendly, ...

$$\sigma^B(q_iq_j \to \tilde{q}\bar{\tilde{q}}) = \frac{\pi\hat{\alpha}_s^2}{s}\left[\beta_{\tilde{q}}\left(-\frac{4}{9}-\frac{4m_-^4}{9(m_{\tilde{g}}^2 s+m_-^4)}\right)+\left(-\frac{4}{9}-\frac{8m_-^2}{9s}\right)L_1\right] + \delta_{ij}\frac{\pi\hat{\alpha}_s^2}{s}\left[\frac{8m_{\tilde{g}}^2}{27(s+2m_-^2)}L_1\right]$$

$$\sigma^B(q\bar{q} \to \tilde{g}\tilde{g}) = \frac{\pi\alpha_s^2}{s}\beta_{\tilde{g}}\left(\frac{8}{9}+\frac{16m_{\tilde{g}}^2}{9s}\right) + \frac{\pi\alpha_s\hat{\alpha}_s}{s}\left[\beta_{\tilde{g}}\left(-\frac{4}{3}-\frac{8m_-^2}{3s}\right)+\left(\frac{8m_{\tilde{g}}^2}{3s}+\frac{8m_-^4}{3s^2}\right)L_2\right] + \frac{\pi\hat{\alpha}_s^2}{s}\left[\beta_{\tilde{g}}\left(\frac{32}{27}+\frac{32m_-^4}{27(m_{\tilde{q}}^2 s+m_-^4)}\right)+\left(-\frac{64m_-^2}{27s}-\frac{8m_{\tilde{g}}^2}{27(s-2m_-^2)}\right)L_2\right]$$

$$\sigma^B(gg \to \tilde{g}\tilde{g}) = \frac{\pi\alpha_s^2}{s}\left[\beta_{\tilde{g}}\left(-3-\frac{51m_{\tilde{g}}^2}{4s}\right)+\left(-\frac{9}{4}-\frac{9m_{\tilde{g}}^2}{s}+\frac{9m_{\tilde{g}}^4}{s^2}\right)\log\left(\frac{1-\beta_{\tilde{g}}}{1+\beta_{\tilde{g}}}\right)\right]$$

$$\sigma^B(qg \to \tilde{q}\bar{\tilde{g}}) = \frac{\pi\alpha_s\hat{\alpha}_s}{s}\left[\frac{\kappa}{s}\left(-\frac{7}{9}-\frac{32m_-^2}{9s}\right)+\left(-\frac{8m_-^2}{9s}+\frac{2m_{\tilde{q}}^2 m_-^2}{s^2}+\frac{8m_-^4}{9s^2}\right)L_3 + \left(-1-\frac{2m_-^2}{s}+\frac{2m_{\tilde{q}}^2 m_-^2}{s^2}\right)L_4\right],$$

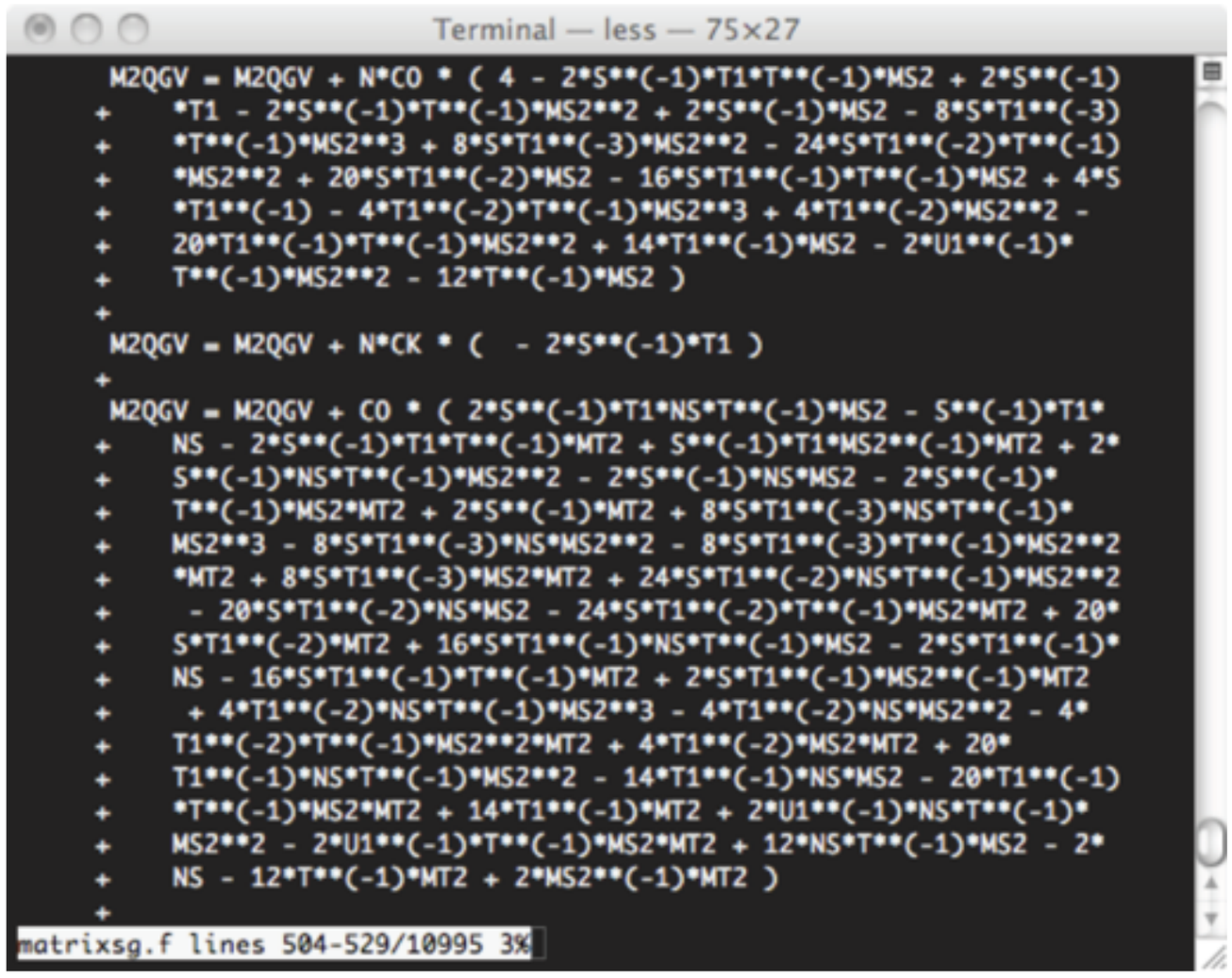

Beyond PROSPINO

- hand-coded, process dependent, user-unfriendly, ...

$$\sigma^B(q_iq_j \to \tilde{q}\bar{\tilde{q}}) = \frac{\pi\hat{\alpha}_s^2}{s}\left[\beta_{\tilde{q}}\left(-\frac{4}{9}-\frac{4m_-^4}{9(m_{\tilde{g}}^2 s+m_-^4)}\right)+\left(-\frac{4}{9}-\frac{8m_-^2}{9s}\right)L_1\right] + \delta_{ij}\frac{\pi\hat{\alpha}_s^2}{s}\left[\frac{8m_{\tilde{g}}^2}{27(s+2m_-^2)}L_1\right]$$

$$\sigma^B(q\bar{q} \to \tilde{g}\tilde{g}) = \frac{\pi\alpha_s^2}{s}\beta_{\tilde{g}}\left(\frac{8}{9}+\frac{16m_{\tilde{g}}^2}{9s}\right) + \frac{\pi\alpha_s\hat{\alpha}_s}{s}\left[\beta_{\tilde{g}}\left(-\frac{4}{3}-\frac{8m_-^2}{3s}\right)+\left(\frac{8m_{\tilde{g}}^2}{3s}+\frac{8m_-^4}{3s^2}\right)L_2\right] + \frac{\pi\hat{\alpha}_s^2}{s}\left[\beta_{\tilde{g}}\left(\frac{32}{27}+\frac{32m_-^4}{27(m_{\tilde{q}}^2 s+m_-^4)}\right)+\left(-\frac{64m_-^2}{27s}-\frac{8m_{\tilde{g}}^2}{27(s-2m_-^2)}\right)L_2\right]$$

$$\sigma^B(gg \to \tilde{g}\tilde{g}) = \frac{\pi\alpha_s^2}{s}\left[\beta_{\tilde{g}}\left(-3-\frac{51m_{\tilde{g}}^2}{4s}\right)+\left(-\frac{9}{4}-\frac{9m_{\tilde{g}}^2}{s}+\frac{9m_{\tilde{g}}^4}{s^2}\right)\log\left(\frac{1-\beta_{\tilde{g}}}{1+\beta_{\tilde{g}}}\right)\right]$$

$$\sigma^B(qg \to \tilde{q}\bar{\tilde{g}}) = \frac{\pi\alpha_s\hat{\alpha}_s}{s}\left[\frac{\kappa}{s}\left(-\frac{7}{9}-\frac{32m_-^2}{9s}\right)+\left(-\frac{8m_-^2}{9s}+\frac{2m_{\tilde{q}}^2 m_-^2}{s^2}+\frac{8m_-^4}{9s^2}\right)L_3 + \left(-1-\frac{2m_-^2}{s}+\frac{2m_{\tilde{q}}^2 m_-^2}{s^2}\right)L_4\right],$$

Terminal — less — 75×27

```
      M2QGV = M2QGV + N*C0 * ( 4 - 2*S**(-1)*T1*T**(-1)*MS2 + 2*S**(-1)
     +     *T1 - 2*S**(-1)*T**(-1)*MS2**2 + 2*S**(-1)*MS2 - 8*S*T1**(-3)
     +     *T**(-1)*MS2**3 + 8*S*T1**(-3)*MS2**2 - 24*S*T1**(-2)*T**(-1)
     +     *MS2**2 + 20*S*T1**(-2)*MS2 - 16*S*T1**(-1)*T**(-1)*MS2 + 4*S
     +     *T1**(-1) - 4*T1**(-2)*T**(-1)*MS2**3 + 4*T1**(-2)*MS2**2 -
     +     20*T1**(-1)*T**(-1)*MS2**2 + 14*T1**(-1)*MS2 - 2*U1**(-1)*
     +     T**(-1)*MS2**2 - 12*T**(-1)*MS2 )
     +
      M2QGV = M2QGV + N*CK * (  - 2*S**(-1)*T1 )
     +
      M2QGV = M2QGV + C0 * ( 2*S**(-1)*T1*NS*T**(-1)*MS2 - S**(-1)*T1*
     +     NS - 2*S**(-1)*T1*T**(-1)*MT2 + S**(-1)*T1*MS2**(-1)*MT2 + 2*
     +     S**(-1)*NS*T**(-1)*MS2**2 - 2*S**(-1)*NS*MS2 - 2*S**(-1)*
     +     T**(-1)*MS2*MT2 + 2*S**(-1)*MT2 + 8*S*T1**(-3)*NS*T**(-1)*
     +     MS2**3 - 8*S*T1**(-3)*NS*MS2**2 - 8*S*T1**(-3)*T**(-1)*MS2**2
     +     *MT2 + 8*S*T1**(-3)*MS2*MT2 + 24*S*T1**(-2)*NS*T**(-1)*MS2**2
     +      - 20*S*T1**(-2)*NS*MS2 - 24*S*T1**(-2)*T**(-1)*MS2*MT2 + 20*
     +     S*T1**(-2)*MT2 + 16*S*T1**(-1)*NS*T**(-1)*MS2 - 2*S*T1**(-1)*
     +     NS - 16*S*T1**(-1)*T**(-1)*MT2 + 2*S*T1**(-1)*MS2**(-1)*MT2
     +      + 4*T1**(-2)*NS*T**(-1)*MS2**3 - 4*T1**(-2)*NS*MS2**2 - 4*
     +     T1**(-2)*T**(-1)*MS2**2*MT2 + 4*T1**(-2)*MS2*MT2 + 20*
     +     T1**(-1)*NS*T**(-1)*MS2**2 - 14*T1**(-1)*NS*MS2 - 20*T1**(-1)
     +     *T**(-1)*MS2*MT2 + 14*T1**(-1)*MT2 + 2*U1**(-1)*NS*T**(-1)*
     +     MS2**2 - 2*U1**(-1)*T**(-1)*MS2*MT2 + 12*NS*T**(-1)*MS2 - 2*
     +     NS - 12*T**(-1)*MT2 + 2*MS2**(-1)*MT2 )
     +
matrixsg.f lines 504-529/10995 3%
```

➡ MadGolem: Fully automated calculation of NLO QCD corrections for arbitrary 2-to-2 processes in generic BSM framework

NLO cross sections

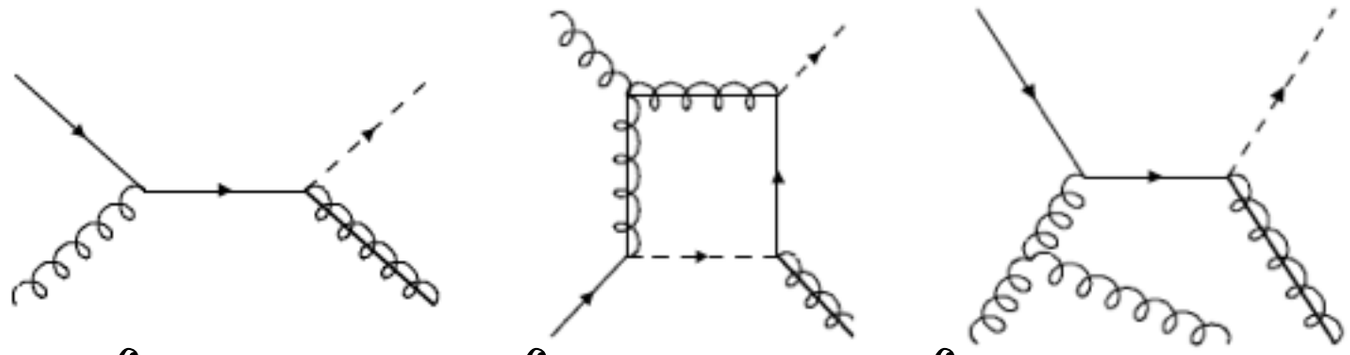

$$\sigma^{NLO} = \int_m d\sigma^B + \int_m d\sigma^V + \int_{m+1} d\sigma^R$$

$$= \int_m d\sigma^B + \int_m [d\sigma^V + \int_1 d\sigma^A] + \int_{m+1} [d\sigma^R - d\sigma^A]$$

$$= \sigma^B + \bar{\sigma}^V + \bar{\sigma}^R$$

NLO cross sections

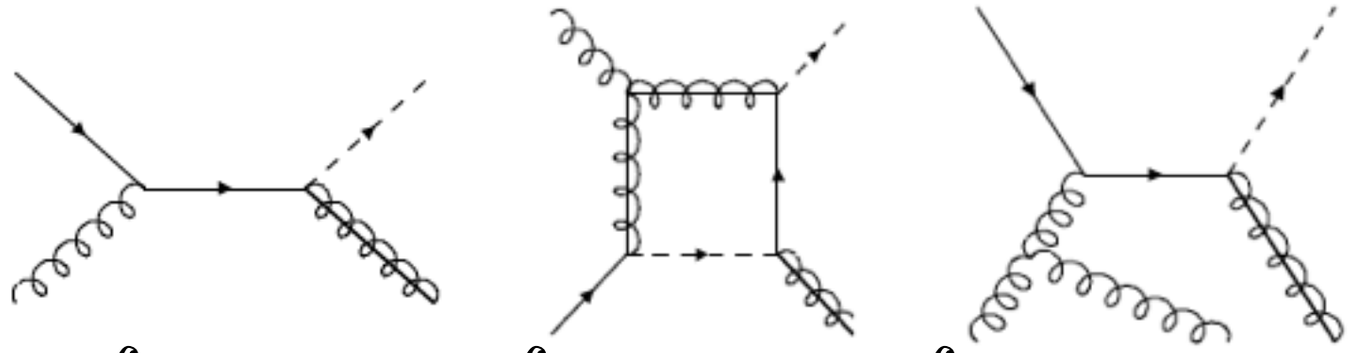

$$\sigma^{NLO} = \int_m d\sigma^B + \int_m d\sigma^V + \int_{m+1} d\sigma^R$$

$$= \int_m d\sigma^B + \int_m [d\sigma^V + \int_1 d\sigma^A] + \int_{m+1} [d\sigma^R - d\sigma^A]$$

$$= \sigma^B + \bar{\sigma}^V + \bar{\sigma}^R$$

$$* \ \bar{\sigma}^V = \left(\frac{c_2}{\epsilon_{IR}^2} + \frac{c_1}{\epsilon_{IR}} + c_0\right) + \left(\frac{c_2'}{\epsilon_{IR}^2} + \frac{c_1'}{\epsilon_{IR}} + c_0'\right) = c_0 + c_0'$$

NLO cross sections

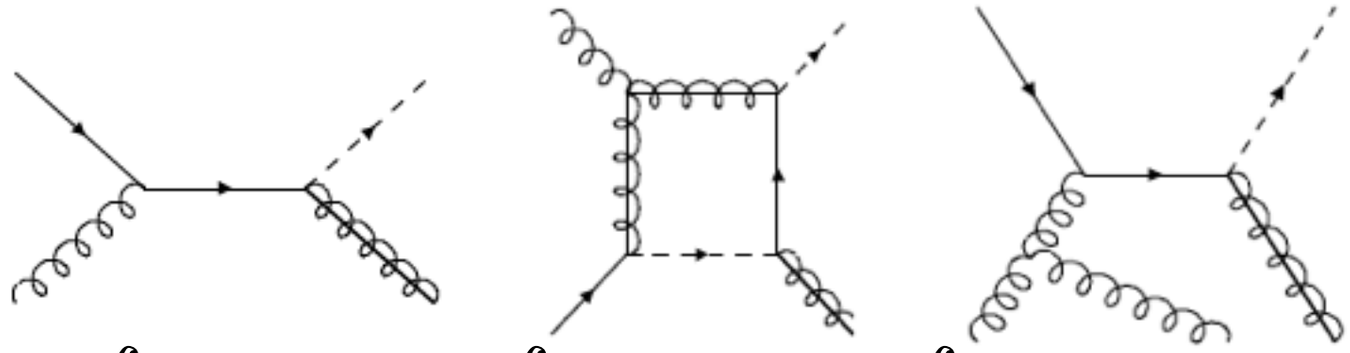

$$\sigma^{NLO} = \int_m d\sigma^B + \int_m d\sigma^V + \int_{m+1} d\sigma^R$$

$$= \int_m d\sigma^B + \int_m [d\sigma^V + \int_1 d\sigma^A] + \int_{m+1} [d\sigma^R - d\sigma^A]$$

$$= \sigma^B + \bar{\sigma}^V + \bar{\sigma}^R$$

$$* \ \bar{\sigma}^V = \left(\frac{c_2}{\epsilon_{IR}^2} + \frac{c_1}{\epsilon_{IR}} + c_0\right) + \left(\frac{c_2'}{\epsilon_{IR}^2} + \frac{c_1'}{\epsilon_{IR}} + c_0'\right) = c_0 + c_0'$$

No IR divergence

→ consistency check of the code

MadGolem

$$\sigma^{NLO} = \int_m d\sigma^B + \int_m [d\sigma^V + \int_1 d\sigma^A] + \int_{m+1} [d\sigma^R - d\sigma^A]$$

MadGolem

MadGraph

$$\sigma^{NLO} = \int_m d\sigma^B + \int_m [d\sigma^V + \int_1 d\sigma^A] + \int_{m+1} [d\sigma^R - d\sigma^A]$$

MadGolem

MadGraph

$$\sigma^{NLO} = \int_m d\sigma^B + \int_m [d\sigma^V + \int_1 d\sigma^A] + \int_{m+1} [d\sigma^R - d\sigma^A]$$

Qgraf+Golem

Feynman-diagram-based method with spinor helicity formalism

- Qgraf: generates loop diagrams
- GOLEM (General One-Loop Evaluator for Matrix elements)

MadGolem

MadGraph

Extended MadDipole

Catani-Seymour dipole subtraction method

$$\sigma^{NLO} = \int_m d\sigma^B + \int_m [d\sigma^V + \int_1 d\sigma^A] + \int_{m+1} [d\sigma^R - d\sigma^A]$$

Qgraf+Golem

Feynman-diagram-based method with spinor helicity formalism

- Qgraf: generates loop diagrams
- GOLEM (General One-Loop Evaluator for Matrix elements)

arXiv:1108.1250

Automized Squark–Neutralino Production to Next-to-Leading Order

Thomas Binoth*,[1] Dorival Gonçalves Netto,[2] David López-Val,[2]
Kentarou Mawatari,[3,4] Tilman Plehn,[2] and Ioan Wigmore[1]

[1]*SUPA, School of Physics & Astronomy, The University of Edinburgh, UK*
[2]*Institut für Theoretische Physik, Universität Heidelberg, Germany*
[3]*Theoretische Natuurkunde and IIHE/ELEM, Vrije Universiteit Brussel, Belgium*
[4]*International Solvay Institutes, Brussels, Belgium*

(Dated: August 8, 2011)

- the first application of the fully automized MadGolem package
  - The one-loop QCD corrections for this process did not yet appear in the literature.
  - potential source of monojet+missE signatures

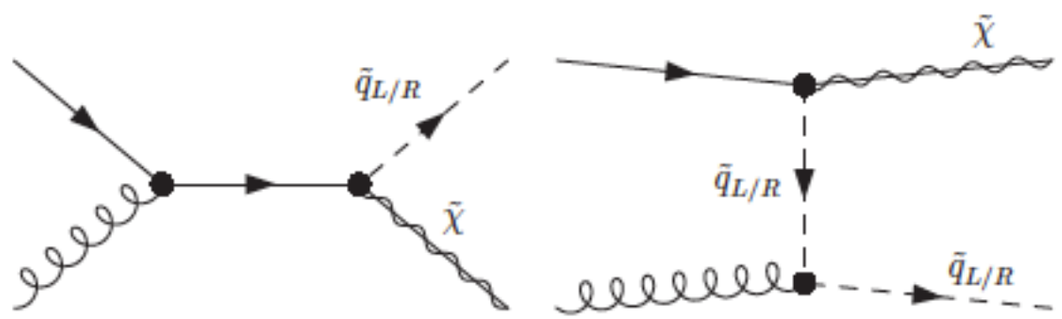

squark-neutralino1 productions

$\sqrt{S}$ [TeV]		$\sigma^{\rm LO}$ [fb]	$\sigma^{\rm NLO}$ [fb]	K		$\sigma^{\rm LO}$ [fb]	$\sigma^{\rm NLO}$ [fb]	K	$m_{\tilde{q}_R}$ [GeV]	$m_{\tilde{q}_L}$ [GeV]
7	$\tilde{u}_R\,\tilde{\chi}_1^0$	29.62	42.17	1.42	$\tilde{u}_L\,\tilde{\chi}_1^0$	0.83	1.26	1.52	549	561
14		176.36	245.74	1.39		5.03	7.52	1.49		
7	$\tilde{d}_R\,\tilde{\chi}_1^0$	3.61	5.31	1.47	$\tilde{d}_L\,\tilde{\chi}_1^0$	1.21	1.77	1.46	545	568
14		24.89	35.50	1.43		8.67	12.37	1.43		
7	$\tilde{c}_R\,\tilde{\chi}_1^0$	1.12	1.81	1.61	$\tilde{c}_L\,\tilde{\chi}_1^0$	0.03	0.06	2.00	549	561
14		13.69	20.69	1.51		0.38	0.66	1.70		
7	$\tilde{s}_R\,\tilde{\chi}_1^0$	0.57	0.78	1.38	$\tilde{s}_L\,\tilde{\chi}_1^0$	0.19	0.29	1.56	545	568
14		5.86	8.45	1.44		2.00	2.98	1.49		
7	$\sum \tilde{q}_R\,\tilde{\chi}_1^0$	34.92	50.07	1.43	$\sum \tilde{q}_L\,\tilde{\chi}_1^0$	2.26	3.38	1.50		
14		220.80	310.38	1.41		16.08	23.53	1.46		

Table I: Individual production rates $\sigma(pp \to \tilde{q}\tilde{\chi}_1^0)$ and corresponding K factors for the modified SPS1a$_{1000}$ scenario. The first and second generation squark masses happen to be degenerate. The scales are set to their central values $\mu_R^0 = \mu_F^0 = (m_{\tilde{q}} + m_{\tilde{\chi}_1^0})/2$. In the last line we show the sum of all contributions.

	$\sqrt{S}$ [TeV]	$\sigma^{\rm LO}$ [fb]	$\sigma^{\rm NLO}$ [fb]	K	$K[\tilde{u}_L]$	$K[\tilde{u}_R]$	$K[\tilde{d}_L]$	$K[\tilde{d}_R]$	$m_{\tilde{u}}$	$m_{\tilde{d}}$	$m_{\tilde{g}}$	$m_{\tilde{\chi}_1^0}$
SPS1a$_{1000}$	7	35.27	50.44	1.43	1.52	1.42	1.46	1.47	$\tilde{u}_L$: 561	$\tilde{d}_L$: 568	1000	97
	14	215.02	301.27	1.40	1.49	1.39	1.42	1.43	$\tilde{u}_R$: 549	$\tilde{d}_R$: 545		
SPS1b	7	2.77	3.99	1.45	1.57	1.43	1.62	1.52	$\tilde{u}_L$: 872	$\tilde{d}_L$: 878	938	162
	14	27.21	37.46	1.38	1.48	1.36	1.52	1.43	$\tilde{u}_R$: 850	$\tilde{d}_R$: 843		
SPS2	7	0.04	0.07	1.52	1.81	1.49	1.69	1.65	$\tilde{u}_L$: 1554	$\tilde{d}_L$: 1559	782	123
	14	1.21	1.64	1.36	1.45	1.34	1.46	1.45	$\tilde{u}_R$: 1554	$\tilde{d}_R$: 1552		
SPS3	7	3.15	4.55	1.44	1.56	1.42	1.59	1.52	$\tilde{u}_L$: 854	$\tilde{d}_L$: 860	935	161
	14	30.20	41.59	1.38	1.49	1.36	1.50	1.43	$\tilde{u}_R$: 832	$\tilde{d}_R$: 824		
SPS4	7	6.44	9.04	1.40	1.52	1.38	1.53	1.49	$\tilde{u}_L$: 760	$\tilde{d}_L$: 766	733	120
	14	52.87	71.40	1.35	1.46	1.33	1.45	1.41	$\tilde{u}_R$: 748	$\tilde{d}_R$: 743		
SPS5	7	13.26	18.11	1.37	1.52	1.40	1.54	1.48	$\tilde{u}_L$: 675	$\tilde{d}_L$: 678	722	120
	14	95.81	132.29	1.38	1.50	1.37	1.49	1.43	$\tilde{u}_R$: 657	$\tilde{d}_R$: 652		

Real and virtual corrections

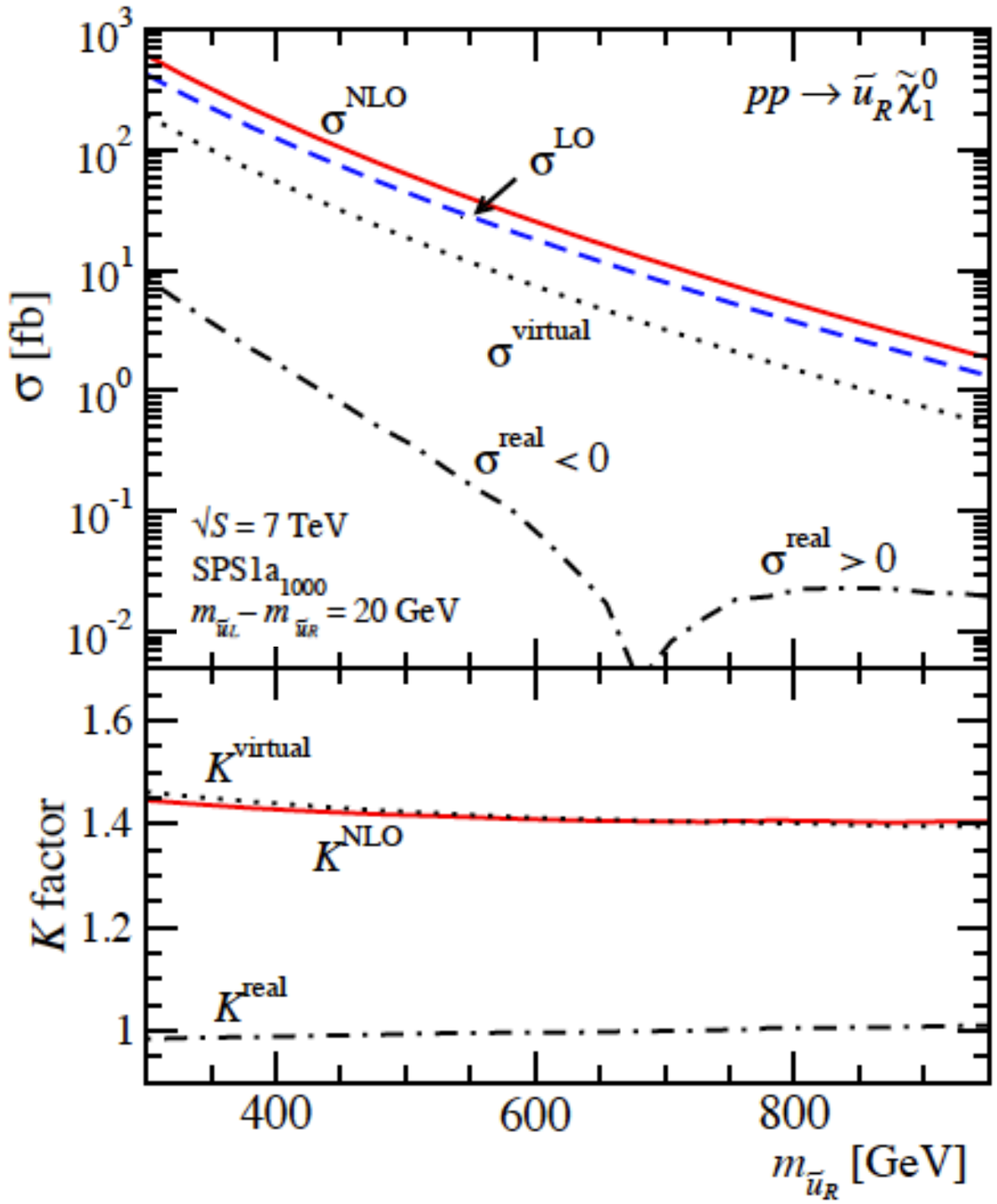

- NLO corrections are insensitive to the squark masses.
- The virtual corrections are dominant.
- $K = \sigma_{NLO}/\sigma_{LO} \sim 1.4$

Structure of the NLO corrections

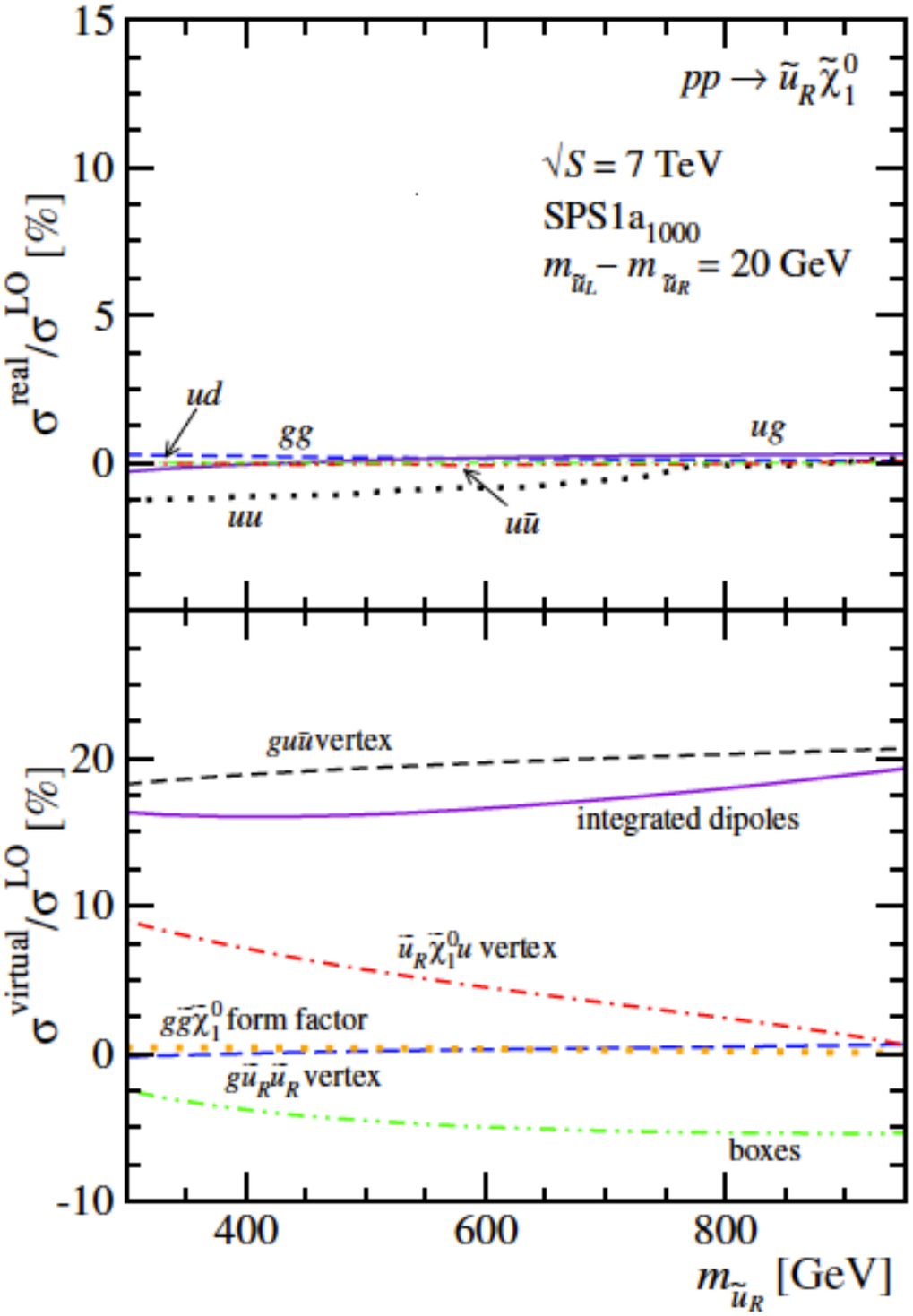

- dominated by pure QCD virtual gluon interchange & real gluon emission.
- SUSY-QCD corrections entail a subleading contribution.

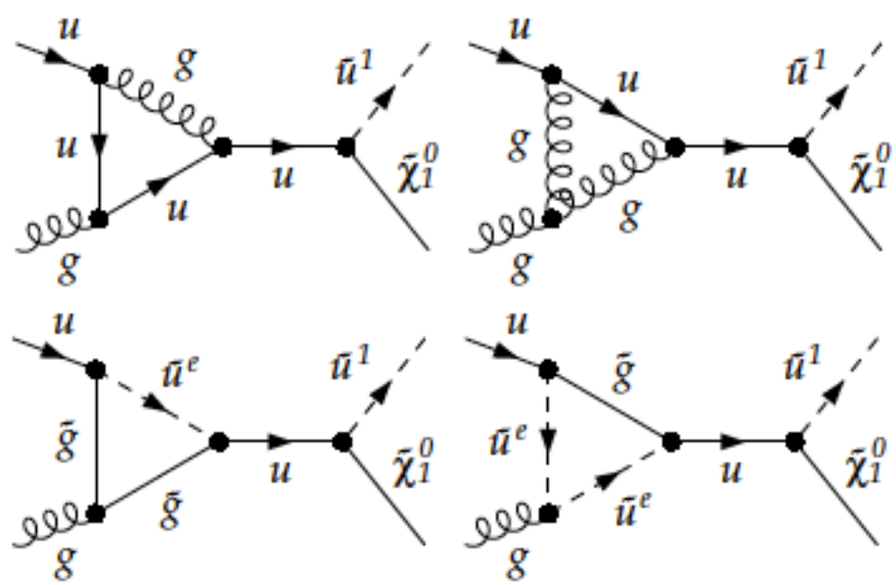

Scale dependences

- One of the main reasons to base LHC analyses on higher-order rate predictions is the stabilization of the dependence on the unphysical renormalization and the factorization scales.

- MadGolem is based on the MG/ME framework, so it is easy to change the scale choices in run_card.dat.

$$\mu^0 = (m_{\tilde{u}} + m_{\tilde{\chi}})/2$$

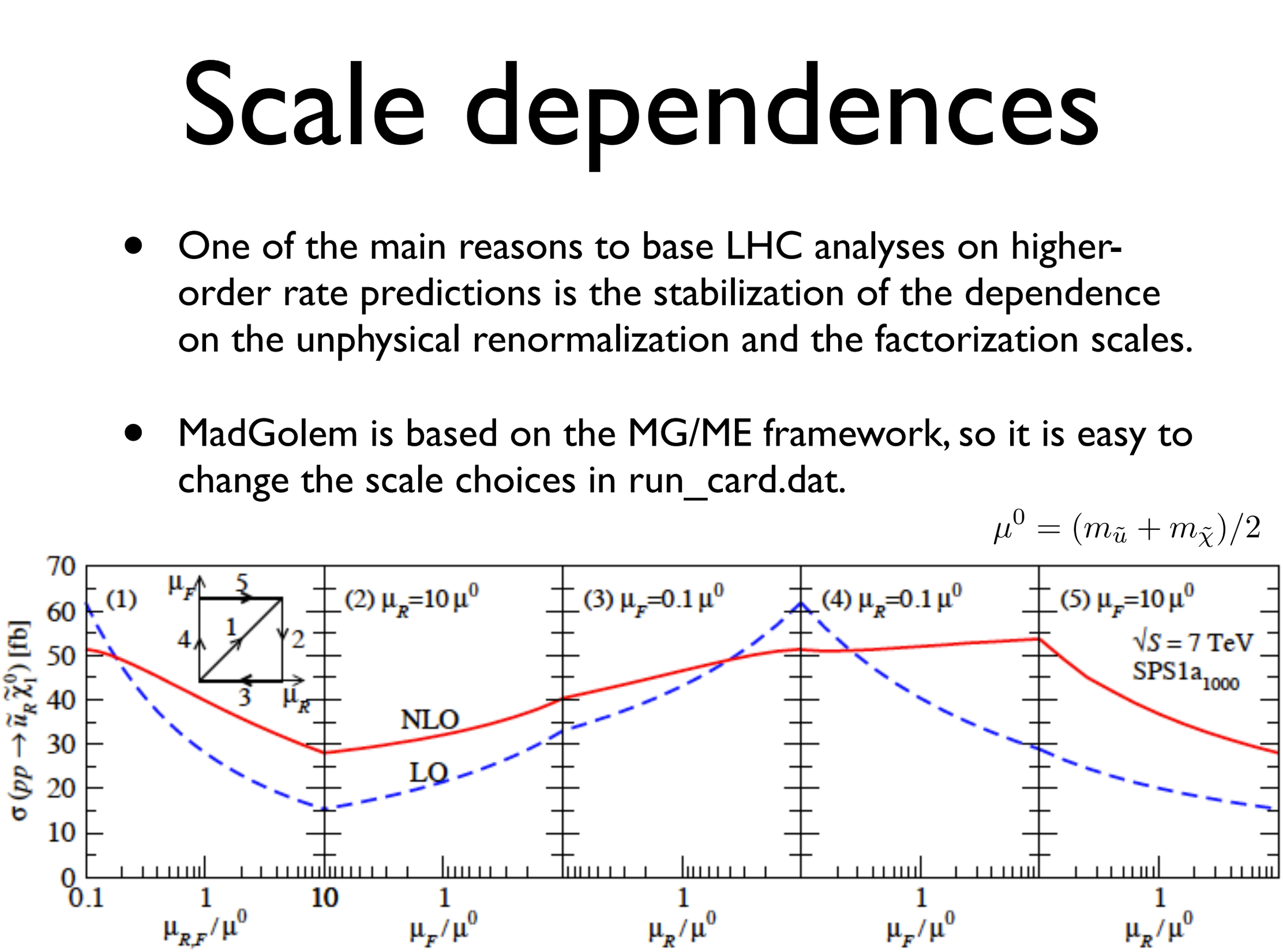

NLO cross section predictions including the scale uncertainty

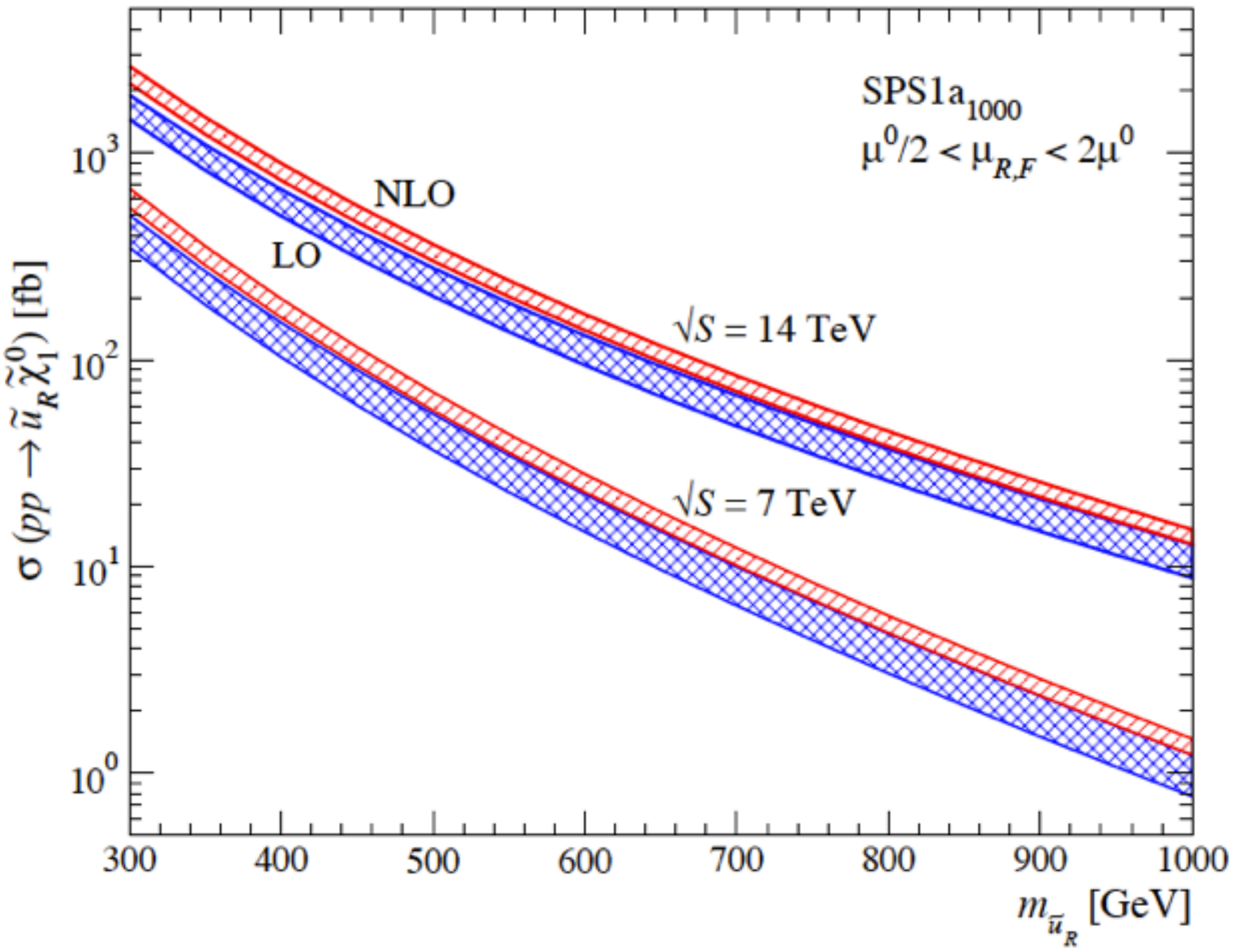

- $\Delta\sigma/\sigma \sim 70\%$ @ LO
- $\Delta\sigma/\sigma \sim 20\%$ @ NLO
- The theory uncertainty is largely reduced.

Summary and outlook

- MadGolem completely automates the calculation of NLO QCD corrections for generic BSM 2-to-2 processes within the MadGraph/Golem framework.
- The squark-neutralino production is the first application, and all SUSY-pair production processes will be publicly available soon.
- To-do-list
  - Alternative BSM models: leptoquark, sgluon, ...
  - MENLOPS matching
  - MadGolem in the MG5 framework
  - ...

Summary and outlook

- MadGolem completely automates the calculation of NLO QCD corrections for generic BSM 2-to-2 processes within the MadGraph/Golem framework.
- The squark-neutralino production is the first application, and all SUSY-pair production processes will be publicly available soon.
- To-do-list
  - Alternative BSM models: leptoquark, sgluon, ...
  - MENLOPS matching
  - MadGolem in the MG5 framework
  - ...